MODELING THREE-DIMENSIONAL SCATTERERS USING A COUPLED FINITE ELEMENT - INTEGRAL EQUATION FORMULATION

Tom Cwik, Cinzia Zuffada, and Vahraz Jamnejad

Jet Propulsion Laboratory

California Institute of Technology

Pasadena CA 91109

Abstract

Finite element modeling has proven useful for accurately simulating scattered or radiated fields from complex three-dimensional objects whose geometry varies on the scale of a fraction of a wavelength. In order to practically compute a solution to exterior problems, the domain must be truncated at some finite surface where the Sommerfeld radiation condition is enforced, either approximately or exactly. This paper outlines a method that couples three-dimensional finite element solutions interior to a bounding surface, with an efficient integral equation solution that exactly enforces the Sommerfeld radiation condition. The general formulation and the main features of the discretized problem are first briefly outlined. Results for far and near fields are presented for geometries where an analytic solution exists and compared with exact solutions to establish the accuracy of the model. Results are also presented for objects that do not allow an analytic solution, and are compared with other calculations and/or measurements.

The research described in this paper was carried out at the Jet Propulsion Laboratory, California Institute of Technology, under a contract with the National Aeronautics and Space Administration.

INTRODUCTION

Finite element modeling has proven useful for accurately simulating scattered or radiated fields from complex three-dimensional objects whose geometry varies on the scale of a fraction of a wavelength. The solution of interior problems-simulating fields in waveguides and cavities–has been successfully accomplished using finite clement methods because a bounding surface, such as the cavity walls, exactly truncates the problem domain. l-he solution of exterior problems–simulating fields scattered or radiated from structures--is more difficult because of the need to numericall y truncate the finite element mesh. To practical y compute a solution to exterior problems, the domain must bc truncated at some finite surface where the Sommerfeld radiation condition is enforced, either approximately or exactly. Approximate methods attempt to truncate the mesh using only local field information at each grid point, whereas exact methods arc global, needing information from the entire mesh boundary. This paper outlines a method that couples three-dimensional finite element (FE) solutions interior to the bounding surface with an efficient integral equation (IE) solution that exactly enforces the Sommerfeld radiation condition.

The problem domain is divided into interior and exterior regions, separated at the mesh boundary. The unknown sources in the integral equation arc directly related to the tangential fields on the mesh boundary, and the radiation condition is implicitly enforced exactly through the use of the free-space Green's function. Fields in the two regions arc coupled by enforcing boundary conditions on tangential field components at the mesh boundary, thereby producing a unique and exact solution to Maxwell's equations in both regions.

The choice of the artificial boundary separating the interior and exterior region has a direct bearing on the solution technique for the exterior region. The selection of a general arbitrary surface allows the mesh to conform to the body and results in the smallest finite element meshing region and hence the smallest FE matrix [1-4,7]. The solution of the integral equation in the exterior region, however, involves the application of a general moment method solution which results in the computer storage and solution lime being at least proportional to

that of a three-ctimensional surface integral equation formulation, defeating the computational efficiency of the finite element method and limiting its usefulness. In the unimoment method introduced by Mci [5], the boundary is the surface of a separable coordinate system (for example the surface of a sphere). In the method introduced by Boyse and Seidl [6] a surface of revolution is proposed which results in eigenfunction series expansion in only one direction (azimuthal).

A complementary issue is the selection of the expansion functions in the finite element and integral equation representations. To enforce continuity of fields across the mesh boundary, the expansion functions used in the integral equation can bc identical or similar to those used at the boundary of the finite element mesh. As mentioned above, this approach leads to the use of a general moment method solution, and in addition to limiting computational efficiency, severely limits the choice and the number of elements of the expansion in the two regions. A second approach decouples the interior finite element mesh from that used for the expansion functions in the integral equation formulation and thus provides flexibility in the choice and number of functions most appropriate to field expansion in each region.

The formulation in [6] employing a surface of revolution boundary, suggested a node-based tetrahedral expansion in the finite element region, and a Fourier modal azimuthal expansion together with Hermite polynomial functions along the surface of revolution generator for the integral equation expansion. A similar two-dimensional formulation for arbitrary scatterers was given in [7]. The genera] three-dimensional formulation in this paper builds upon the previous works [6,7], following [6] in the use of a surface of revolution to truncate the finite element mesh. The work in this paper utilizes vector edge elements to discretize the Helmholtz wave equation, and piecewise triangle functions along the generator to efficiently model the mesh truncation surface. The vector edge elements naturally enforce the boundary condition at perfectly conducting surfaces and do not allow the generation of parasitic fields encountered when applying nodal elements. They also produce fewer non-zero entries in the resultant sparse system of equations relative to nodal elements. This approach has broad applicability in

modeling both the near and far fields as shown by the extensive set of calculations presented in this paper. A complete, and detailed description of this formulation is given in [8].

The formulation has also been extended to radiation problems (e.g., antenna elements or arrays) by correctly modeling impressed sources within the finite element mesh. The radiation modeling is reported in [9].

THEORETICAL FORMULATION

The scatterer and surrounding space arc broken into two regions: an interior part containing the scatterers and freespace region out to a defined surface, and the exterior homogenous part (Figure 1).

The Finite Element Representation

In the interior region, a finite element discretization of a weak form of the wave equation is used to model the geometry and fields, leading to

$$\frac{\eta_0}{jk_0}\iiint_V \left[\frac{1}{\varepsilon_r}(\nabla\times\vec{H})\bullet(\nabla\times\vec{W}^*)-k^2\mu_r\vec{H}\bullet\vec{W}^*\right]dv-\iint_{\partial V}\vec{E}\times\hat{n}\bullet\vec{W}^*ds=0 \qquad (1)$$

$\vec{H}$ is the magnetic field (the }~-equation is used in this paper; a dual fi-equation can also be written), $\vec{W}$ is a testing function, the asterisk denotes conjugation, and $\vec{E}\times\hat{n}$ is the tangential component of $\vec{E}$ on the surface of revolution S (∂V). Equation (1) represents the fields internal to and on the surface S. These fields will bc modeled using a set of properl y chosen finite element basis functions. I n Equation (1), ε_r and μ_r arc the relative permittivity and permeability respectively, and k_0 and η_0 arc free-space wave number and impedance, respectively.

The Combined-Field Integral Equation Representation

in the formulation of the integral equation, fictitious electric $\left(\bar{J} = \hat{n} \times \bar{H}\right)$ and magnetic $\left(\bar{M} = -\hat{n} \times \bar{E}\right)$ surface currents, equivalent to the tangential magnetic and electric fields just on the exterior of the boundary surface, arc defined on the boundary. These currents produce the scattered fields in the exterior region. A linear combination of the electric field integral equation (EFIE) and the magnetic field integral equation (MFIE) is used in this formulation, and it can be succinctly expressed as

$$Z_M[\bar{M}/\eta_0] + Z_J[J] = V_i \tag{2}$$

where Z_M and Z_J arc the intcgro-differential operators used in defining the CFIE, and V_i represents the incident field.

Enforcing Boundary Conditions

At the artificial surface of revolution separating the interior and exterior regions, boundary conditions on the continuity of tangential field components must be enforced. Three equations arc written for the three unknown field quantities of interest, the magnetic field $\bar{H}$ internal to the volume V and the electric and magnetic surface currents, $\bar{J}$ and $\bar{M}$, on the boundary. Continuity of the magnetic field across the boundary is enforced in a weak sense

$$\iint_{\partial N} \left(\hat{n} \times \bar{H} - \bar{J}\right) \bullet (\hat{n} \times \bar{U}^*) ds = 0 \tag{3}$$

where $\bar{U}$ is a testing function. This is an essential boundary condition and must be explicitly enforced. Continuity of the electric field across the boundary is made implicit in the finite element equation in the surface integral term $\hat{n} \times \bar{E}$, by replacing this term with M, and is termed a natural boundary condition.

NUMERICAL IMPLEMENTATION

The above three equations are discretized using appropriate sets of basis functions. In the interior region, tetrahedral, vector edge elements (Whitney elements) are used,

$$\overline{W}_{mn}(r) = \lambda_m(r)\nabla\lambda_n(r) - \lambda_n(r)\nabla\lambda_m(r) \tag{4}$$

in which $\lambda(r)$ are the tetrahedral shape functions and indices (m,n) refer to the two end points of each edge. These elements are used for both expansion and testing (Galerkin's method) in the finite element domain.

For the integral equation on the surface of revolution, again applying Galerkin's method, a set of basis functions with piecewise linear variation along the surface of revolution generator, and with an azimuthal Fourier modal variation are used. Thus both expansion and testing functions are given as

$$\begin{bmatrix} \overline{U}^{t} \\ \overline{U}^{\phi} \end{bmatrix} = \begin{bmatrix} \hat{t} \\ \hat{\phi} \end{bmatrix} \frac{T_k(t)}{\rho(t)} e^{jn\phi} \tag{5}$$

in which $T_k(t)$ is a triangle function spanning the k-th annulus on the surface of revolution surface. The variables t and ϕ refer to the local surface of revolution coordinates, and ρ is the distance from the z-axis to a point on the surface of revolution. Each annulus spans two segments along the generator, each referred to as a strip. Adjacent triangles overlap on one segment. The formulation is similar to the one used in the development of the CICERO code[10], although other similar formulations are also possible.

The surface integral in (1) and the first component of the integral in (3) are termed the coupling integrals, since with a convenient choice of the unknown in the first and of the testing function in the second, they are made to couple interior and exterior field representations.

To evaluate these terms, the FE basis function $\overline{W}$ is evaluated approximately on the portion of surface of revolution projected from the triangular facet of the tetrahedron onto a strip. Such projections are curved triangles, curved quadrilaterals, or curved pentagons. The evaluation of the integrals was done numerically. These coupling integrals, as well as the discretization of the second surface integral in (3), complete the discretization of the problem.

NUMERICAL SOLUTION OF THE I.INItAI< SYSTEM

Having introduced the basis and testing functions for the volume as well as the surface unknowns, substitution into the complete set of equations ields

$$\begin{vmatrix} K & C & o \\ C^{\dagger} & o & Z_0 \\ 0 & Z_M & Z_J \end{vmatrix} \begin{vmatrix} H \\ M \\ J \end{vmatrix} = \begin{vmatrix} 0 \\ 0 \\ VI \end{vmatrix} \tag{6}$$

$$\begin{aligned} \mathbf{K} &= \left\langle K_p \left[\bar{T}_p \right] \cdot \bar{T}_q \right\rangle \\ \mathbf{C} &= -\eta_0 \left\langle \bar{U}_m \cdot \bar{T}_q \right\rangle \\ \mathbf{Z_0} &= \eta_0 \left\langle \bar{U}_m \cdot \left[\hat{n} \mathrm{x} \bar{U}_n \right] \right\rangle. \\ \mathbf{Z_M} &= \left\langle Z_{Mm} \left[\bar{U}_m \right] \bar{U}_n \right\rangle \\ \mathbf{Z_J} &= \left\langle Z_{Jm} \left[\bar{U}_m \right] \cdot \bar{U}_n \right\rangle \end{aligned} \tag{7}$$

The symbol † indicates (he adjoint of a matrix. Note that both **K** and C arc sparse, $\mathbf{Z_0}$ is tri-diagonal and $\mathbf{Z_M}$ and $\mathbf{Z_J}$ are banded. In particular the system is complex, non-symmetric, and non-Hermitian.

The solution to this matrix equation has been developed using two alternative strategies depending upon the application. The two approaches arc

1) Solve the entire system in one step using an iterative algorithm for non-symmetric systems. In this work the non-symmetric variant of the quasi-minima! residual (QMR) algorithm [11,12] was applied.

2) Solve the system in two steps by first eliminating 11 through the computation of $\mathbf{Z_K} = \mathbf{C}^{\dagger} \mathbf{K}^{-1} \mathbf{C}$ and then by solving the reduced system

$$-\mathbf{Z}_K\mathbf{M} + \mathbf{Z}_0\mathbf{J} = \mathbf{0}$$
$$\mathbf{Z}_M\mathbf{M} + \mathbf{Z}_J\mathbf{J} = \mathbf{V}_i \tag{8}$$

The first step was accomplished by applying a symmetric variant of the QMR iterative algorithm or a direct solver based on an sparse LDL^t factorization. The resulting overall matrix (8) was treated as being dense, and the solution of this second system was accomplished via a direct dense LU decomposition, since its size is relatively small.

The choice of the solution method is dependent upon a variety of factors, including the number of right-hand side (RHS) excitation vectors and the efficacy of a preconditioner if iterative algorithms are used to calculate $\mathbf{Z}_K$ in the second method. The computational cost of the first method is mainly due to solving the system iteratively for each RHS. The major computational cost in the second method is calculating $\mathbf{Z}_K$; this requires the solution of a system of equations, $\mathbf{K}^{-1}\mathbf{C}$, where C is a rectangular matrix with a possibly large number of columns for electrically large scatterers. When considering a radiation problem where there are one or a few right-hand sides, or a scattering problem with one or a few excitations, the first method may be preferable. When mono-static RCS calculations are performed and there are upwards of thousands of right-hand sides, the second method is more efficient. This second approach has been implemented on scalable distributed memory computers, and is reported in [13].

NUMERICAL RESULTS

Several scatterers have been examined in detail, including dielectric spheres, finite length (coated) metal cylinders, rectangular concspheres, including one with a groove near the cone-sphere boundary, and metal cubes. The features of some of the meshes are shown in Table 1. A surrounding shell is used to model a perfectly conducting object coated with a layer of dielectric material. As a special case, by choosing the dielectric coating to be air, the scattering from the perfectly conducting object itself is obtained. Naturally, no elements are required to model fields

inside perfect conductors. The choice of metallic objects was based on the existence of results from other available codes or measurements.

Table 1. Objects and their mesh densities

Object	Nodes	Elements	Edges
Dielectric sphere	865	3963	5217
Metal cylinder (coated)	8012	24246	40476
Metal conesphere	8882	31485	47192
Metal conesphere with groove	4742	15641	24492
Metal cube	15401	73677	94288

When considering the dielectric sphere, only the scatterer itself was modeled by the mesh since there is no need to extend the mesh outside the geometry of the scatterer. In the case of the metal cylinder (height/dianlctcr = 1.92) the mesh was a shell conforming to the object with a thickness chosen to fit onc tetrahedral element edge only, keeping the volume of the region around the recta] scatterer to a minimum. The problem of a metal cylinder coated with a dielectric material is also treated with this choice of mesh.

The metal conespheres were modeled with a quasi-conforms] mesh, i.e., it has the same geometry as the object everywhere except in a region c1osc to the tip, where the mesh (unlike the object) does not come to a point. An illustration of one-quarter of the conesphere mesh, cut along the longitudinal axis in Figure 2. This plot illustrates that two different edge lengths were chosen to properly model the geometry of the tip of the conical section, as well as the field variation in the volume around it, while retaining a much larger edge length in the mesh volume around the hemispherical portion. The conesphere had a cone ha] f-angle of 20°, a hemispherical cap diameter of 2.54 cm, and a conical section length of 3.74 cm. It is selected from a set of measured objects currently available.

The metallic cube was enclosed in a cylindrical shell of free space which was designed to be big enough to accommodate onc or two tetrahedra (radially) in the regions between the

corners of the cube and (he terminating surface of revolution. Therefore, with a cube side of 1 cm, the radius of the cylinder was taken to bc 0.8 cm.

RCS and Near-Field Results

A set of RCS calculations, showing comparisons with either analytical results or with calculations obtained with the CICERO code, or measurements, is provided in Figs. 3-8. In the legend calculations by this method arc referred to as *PHOEBUS*, the name of the scattering code developed in this work. Figure 3 refers to the case of a metal cylinder (height = 10 cm, radius = 2.6 cm) coated with a layer of dielectric (ε_r=3) at a frequency of 3 GHz; the thickness of the layer is 0.2 cm, i.e. 0.035 wavelength in the dielectric. Comparisons arc made with results from CICERO.

Figure 4 shows the monostatic RCS of a metal conesphere (cone half angle = 20°, sphere diameter = 2.54 cm) in the E-plane (horizontal polarization). At the frequency of 14 GHz the height of the scatterer is 2.3 wavelengths. Note that the ϕ = 0(' direction corresponds to the middle of the hemispherical cap whereas the ϕ = 180° direction is the tip of the conical section. Comparisons arc provided with measured data as well as with calculations obtained with the CICERO code. Figure 5 illustrates the monostatic RCS of the conesphere with a groove located as shown in the inset of the figure. The excitation frequency is 10 GHz. This conesphere geometry except for the groove is identical to that of Figure 4. The monostatic RCS for this object is compared to that of the CICERO result, and for comparison, the RCS of the same conesphere without groove is shown on the same figure. RCS differences with and without the groove arc therefore highlighted in this plot. Figure 6 illustrates the RCS results for a metal cube (side = 1 cm) at a frequency of 22.5 GHz compared with existing measurements [14] and calculations from the PATCH integral equation code [15]. The incident direction is taken to bc normal to a face.

Figures 7 and 8 illustrate near-field results computed within the finite clement mesh. Figure 7 is a plot of the total magnetic field magnitude inside a dielectric sphere in the direction

specified by the equation (y=0, z= O), i.e., a line parallel to the x-axis. The sphere radius was 1 cm and the frequency 5 GHz. The small discontinuities in the curve. arc duc to slight variations in the field components normal to an element face when transitioning from one tetrahedron to an adjacent one. The nominal value of the edge length was 1/20th of the corresponding wavelength inside the dielectric. Figure 8 is a plot of the tangential phi component of $\overline{H}$ on a metal cylinder of length 10 cm and radius 2.6 cm. The frequency is 2 GHz, and the excitation field is incident normal to the bottom end cap of the cylinder. Shown in this figure arc fields on the bottom and top end caps, and along the straight section of the cylinder. The local coordinates of each of the three sections is shown. The set of results on the left arc from the 1'1101 3BUS code and those on the right arc from CICERO. The scale indicates the magnitude of the magnetic field for an incident field magnitude of 1 A/cm. The structure of the nulls in the field and the relatively strong fields on the bottom cap compared to the top cap are readily apparent.

CONCLUSIONS

" This paper presents a method to compute the fields of penetrable three-dimensional scatterers of general shape by coupling a finite clement solution to an integral equation solution on a surface of revolution. The surface of revolution is chosen to surround the scatterer, resulting in a minimal amount of volume that needs to be discretized. The usc of the integral equation provides an exact enforcement of the Sommerfeld radiation condition. Vector edge elements arc used to discretize the fields inside the volume, whereas the integral equation is discretized on a decoupled surface mesh, introducing a small set of additional basis functions to the system. A software package named PHOEBUS was developed, and used to simulate the scattered fields for a variety of objects, as well as fields inside penetrable scatterers and on metal surfaces.

ACKNOWLEDGMENT

The authors wish to gratefully acknowledge Jean Patterson, manager of the task *Research in Parallel Computational Electromagnetics*. *The* authors also wish to thank S. Misra and C. Larose of the Defense Research Establishment of Ottawa, Canada for providing the measured RCS of the conesphere in Figure 4.

REFERENCES

[1] J.-M. Jin and V. Liepa, "Application of Hybrid Finite Element Method to Electromagnetic Scattering from Coated Cylinders," *IEEE Trans. Antennas and Propagat. ion, vol. AP-36,* pp. 50--54, Jan. 1988.

[2] R. Calalo et al., "Hypercube Matrix Computation Task, Research in Parallel Computational Electromagnetics, Report for 1988 -1989," Jet l'repulsion Laboratory, Nov. 1989.

[3] Z. Gong and A. Glisson, "A Hybrid Equation Approach for the Solution of Electromagnetic Scattering Problems involving Two-Dimensional Inhomogenous Dielectric Cylinders," *IEEE Trans. Antennas Propagat., vol. AP-38*, pp. 60-68, Jan. 1990.

[4] X. Yuan, D. Lynch, and J. Strohbehn, "Coupling of finite element and moment methods for electromagnetic scattering from inhomogenous objects," *IEEE Trans. Antennas Propagat., vol. AP-38*, pp. 386–394, Mar. 1990.

[5] K. K. Mci, "Unimoment method of solving antenna and scattering problems," *IEEE Transactions on Antennas and Propagat., vol. AP-22,* pp. 760--766, Nov. 1972.

[6] W. Boyse and A. Seidl, "A Hybrid Finite Element Method for Near Bodies of Revolution," *IEEE Trans. Mag, vol.* 27, pp. 3833-3836, Sept. 1991.

[7] 'l'. Cwik, "Coupling Finite Element and Integral Equation Solutions Using Decoupled Boundary Meshes," *IEEE Trans. Antennas Propagat., vol. AP-40, no. 12,* pp. 1496-1504, Dec. 1992.

[8] T. Cwik, C. Zuffada, and V. Jamnejad "Efficient Coupling of Finite Element and Integral Equation Representations for Three-Dimensional Modeling," *Finite Element Software for Microwave Engineering,* T. Itoh, G. Pelosi, P. Silvester, Editors, John Wiley and Sons, Inc., to be published Summer 1996.

[9] C. Zuffada, T. Cwik, and V. Jamnejad, "Modeling Radiation with an Efficient Hybrid Finite Element-Integral Equation-Waveguide Mode Modeling Technique," Submitted to IEEE Transactions on Antennas and Propagation, 1995.

[10] L. N. Medgeysi-Mitschang and J. M. Putnam, "Electromagnetic Scattering from Axially Inhomogeneous Bodies of Revolution," *IEEE Transactions on Antennas and Propagation, vol. AP-32,* pp. *797–806,* 1984.

[11] R. W. Freund and N. M. Nachtigal, "QMR: a Quasi-Minimal Residual Method for Non-Hermitian Linear Systems," *Numerische Mathematik, 60,* pp. 315-339, 1991.

[12] E. Lucas, Personal Communications.

[13] T. Cwik, D. Katz, C. Zuffada, and V. Jamnejad, "The Application of Scalable Distributed Memory Computers to the Finite Element Modeling of Electromagnetic Scattering and Radiation," submitted to Computer Methods in Applied Mechanics and Engineering, 1995.

[14] M. Cote, M. Woodworth, and A. Yaghjian, "Scattering from the Perfectly Conducting Cube," *IEEE Transactions on Antennas and Propagation, AP-36,* pp. 132 1–1 329, Sept. 1988.

[15] W. Johnson, D. R. Wilton, and R. M. Sharpe, "Modeling Scattering From and Radiation by Arbitrary Shaped Objects With the Electric Field Integral Equation Triangular Surface Patch Code", *Electromagnetics, vol. 10,* pp. 41 -64, Oct. 1990.

LIST OF FIGURES

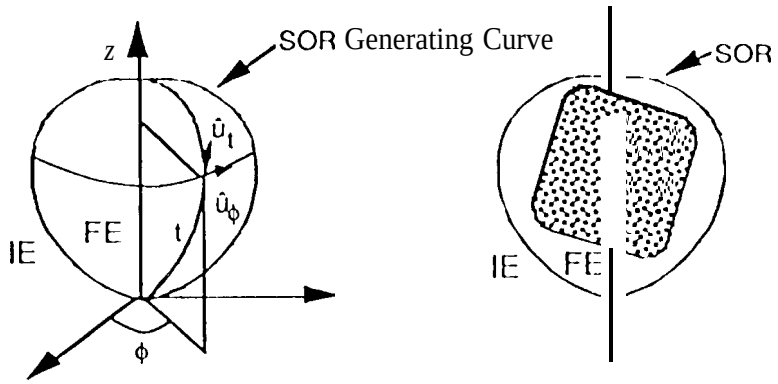

Figure 1. Geometry of scatterer showing intro ior and exterior regions

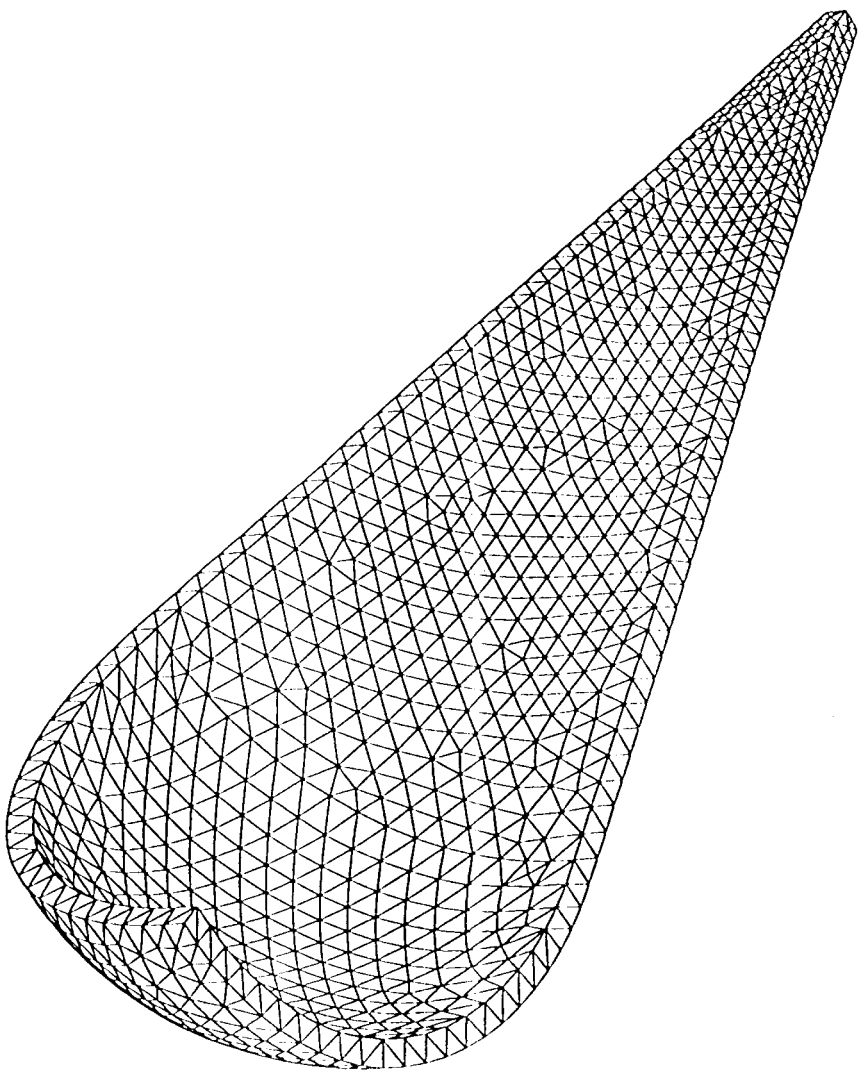

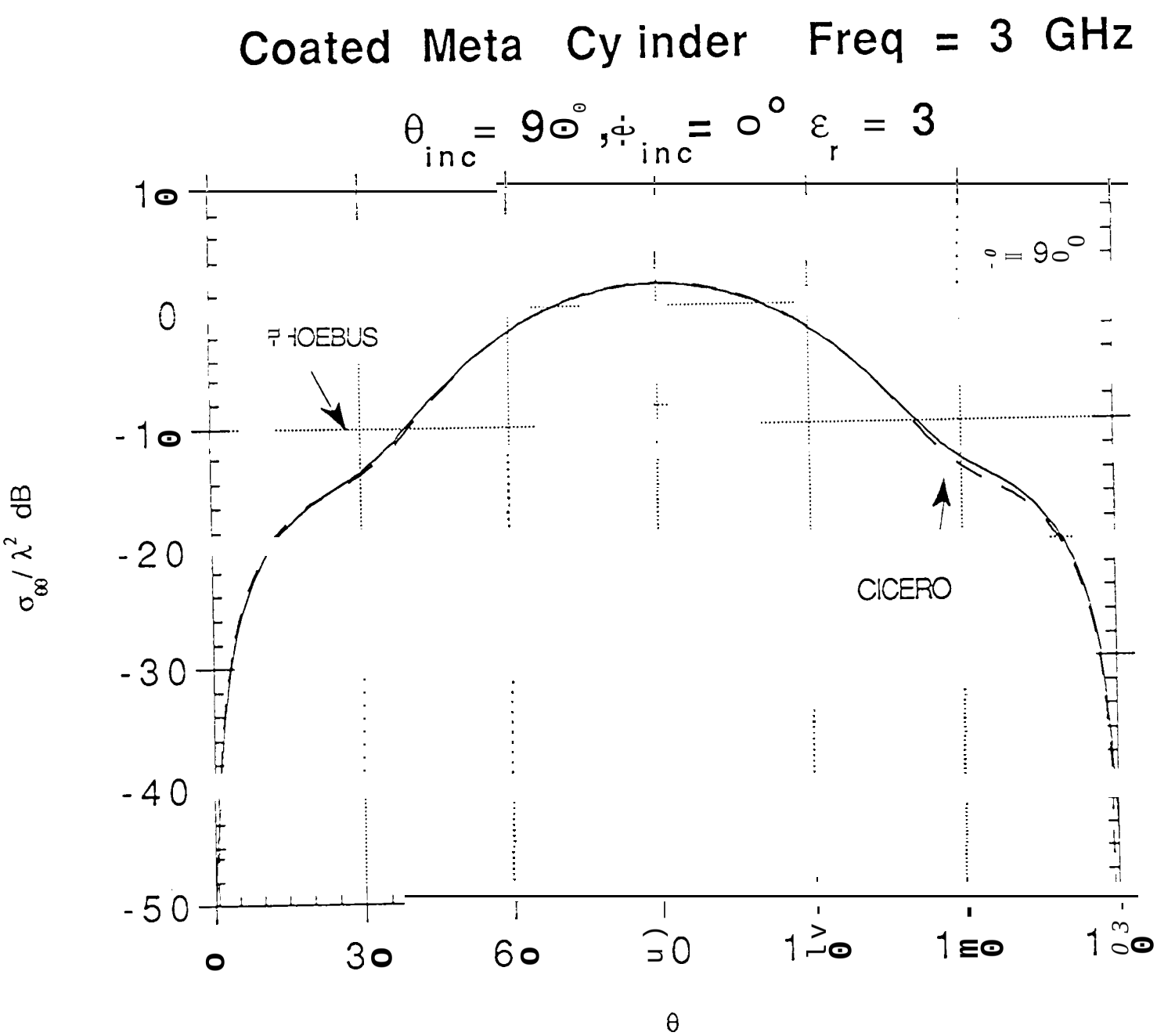
Coated Meta Cy inder Freq = 3 GHz
θ inc = 9o° ,φ inc = o° εr = 3
1o
0
-1o
-20
-30
-40
-50
σ∞/λ² dB
PHOEBUS
CICERO
o
3o
6o
θ

Canadian Space Agency Conesphere
Freq = 14 GHz Monostatic RCS

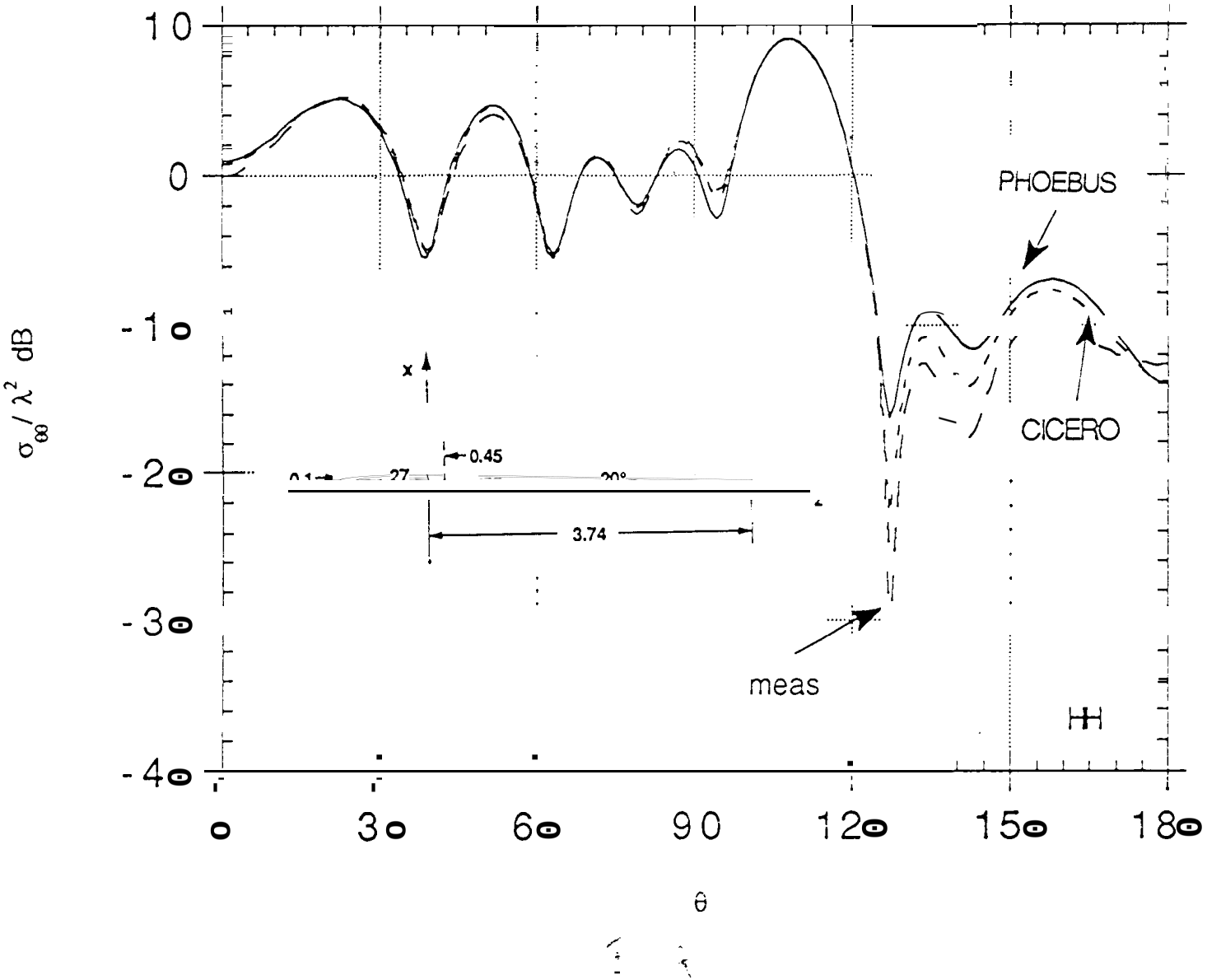

Conesphere with and without groove
Freq = 10 GHz Monostatic RCS

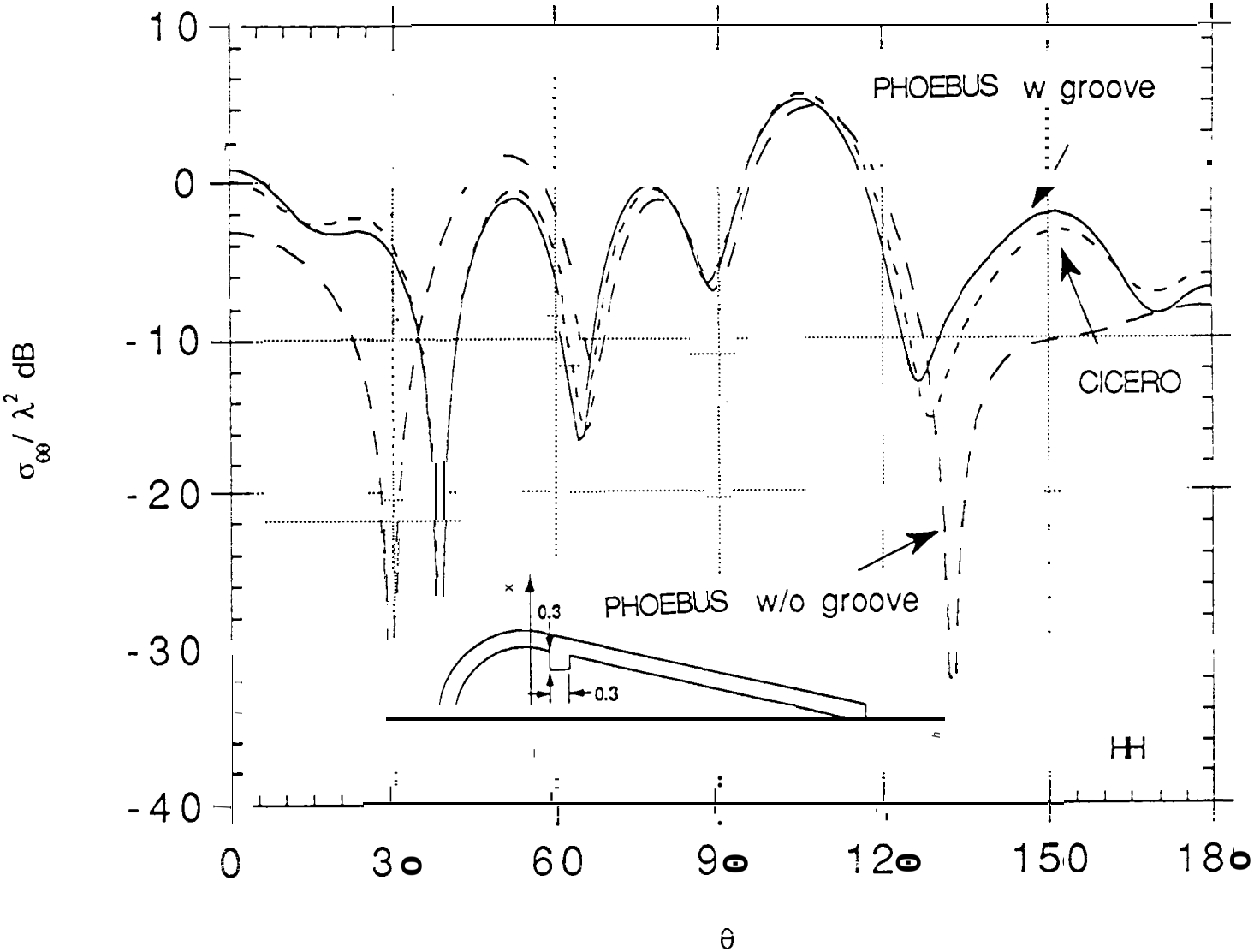

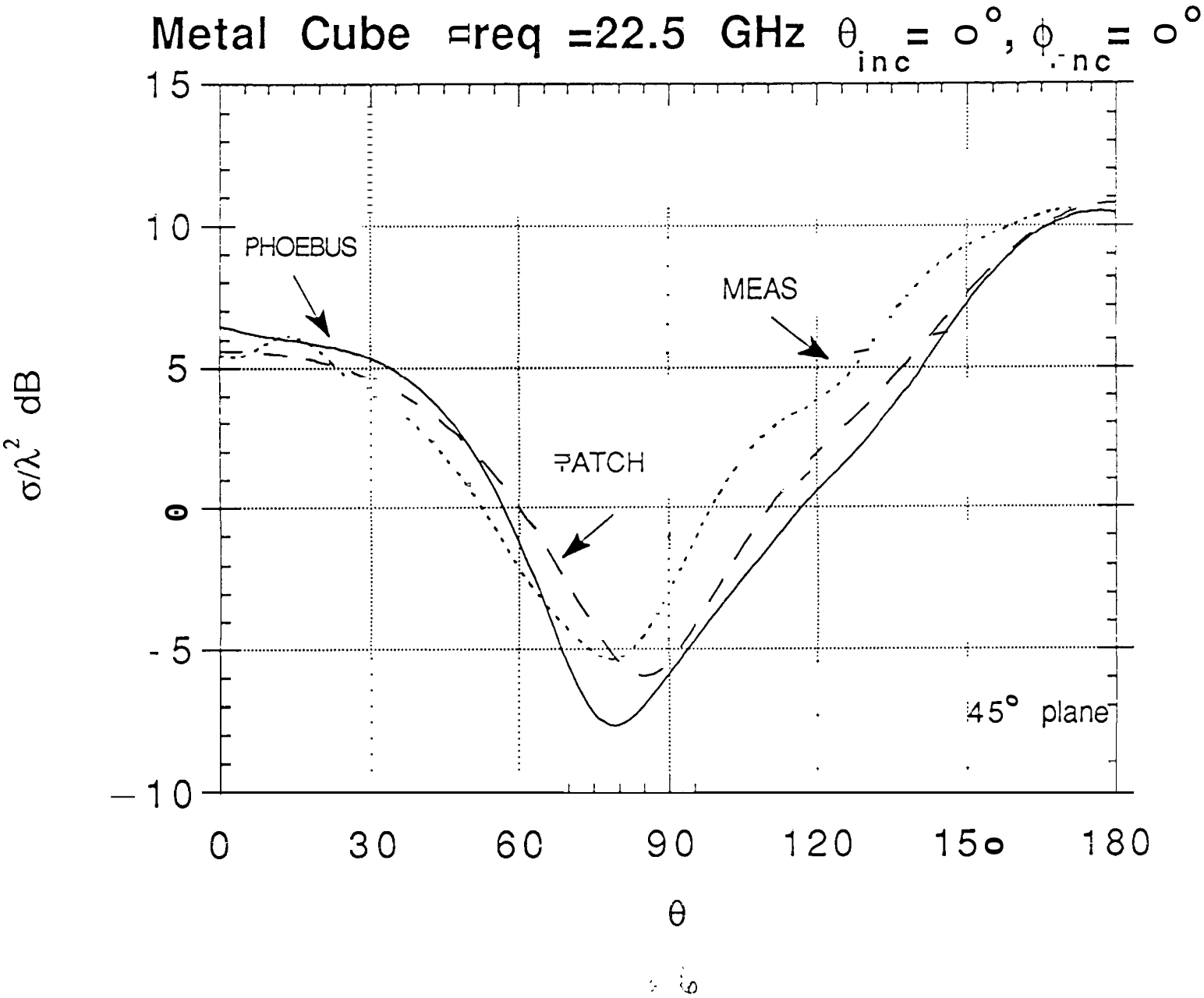
Metal Cube Freq =22.5 GHz θinc = 0°, φinc = 0°
15
10
5
0
-5
-10
σ/λ² dB
PHOEBUS
MEAS
PATCH
45° plane
0
30
60
90
120
150
180
θ

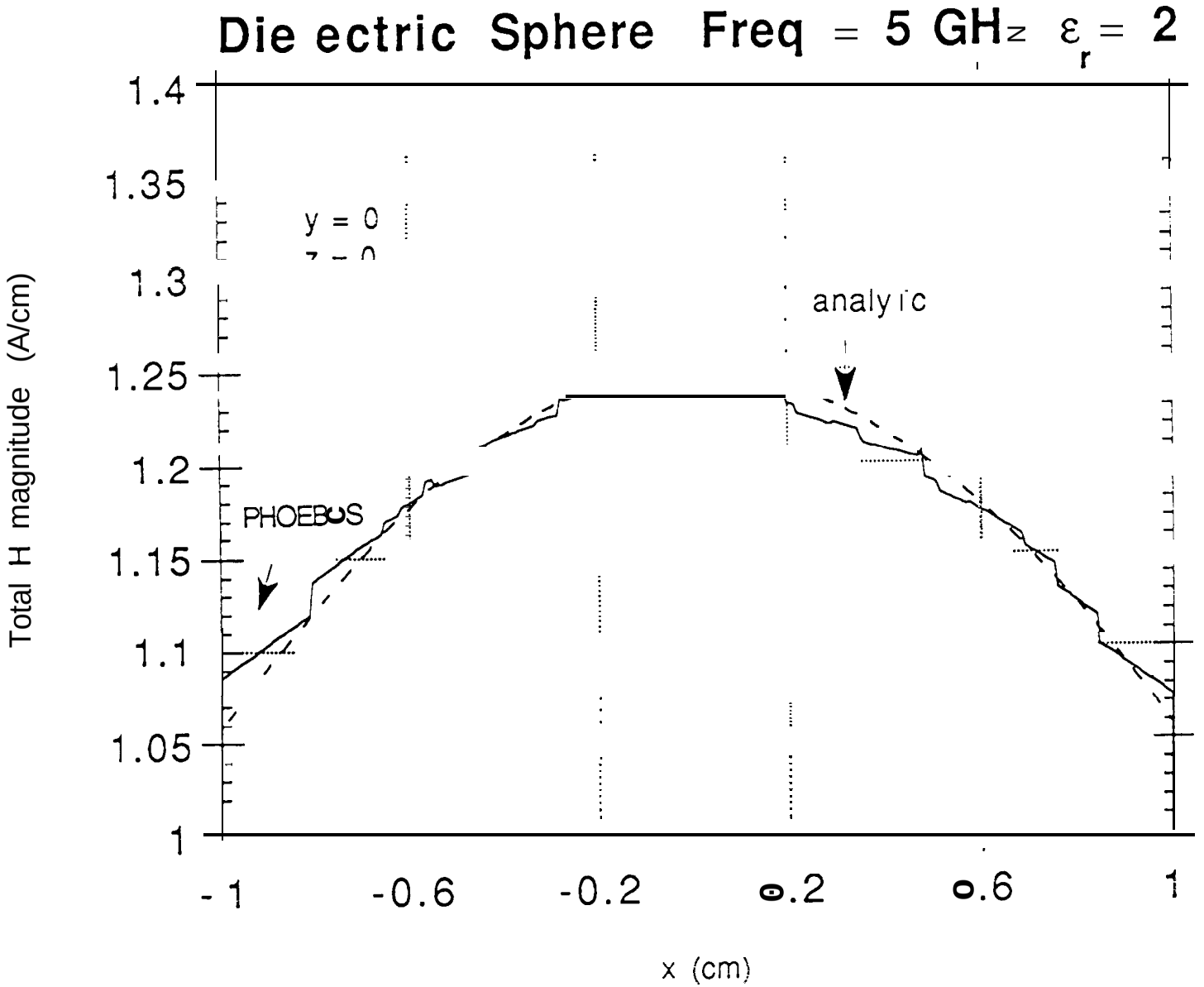
Die ectric Sphere Freq = 5 GHz ε_r = 2
1.4
1.35
1.3
1.25
1.2
1.15
1.1
1.05
1
y = 0
analytic
PHOEBUS
Total H magnitude (A/cm)
-1
-0.6
-0.2
0.2
0.6
1
x (cm)

Fig 3

TANGENTIAL Hϕ ON METAL SURFACE